Predataxis behavior in *Myxococcus xanthus*

James E. Berleman, Jodie Scott, Tatiana Chumley, and John R. Kirby[1]

Department of Microbiology, University of Iowa, 51 Newton Road, Iowa City, IA 52242

Spatial organization of cells is important for both multicellular development and tactic responses to a changing environment. We find that the social bacterium, *Myxococcus xanthus* utilizes a chemotaxis (Che)-like pathway to regulate multicellular rippling during predation of other microbial species. Tracking of GFP-labeled cells indicates directed movement of *M. xanthus* cells during the formation of rippling wave structures. Quantitative analysis of rippling indicates that ripple wavelength is adaptable and dependent on prey cell availability. Methylation of the receptor, FrzCD is required for this adaptation: a *frzF* methyltransferase mutant is unable to construct ripples, whereas a *frzG* methylesterase mutant forms numerous, tightly packed ripples. Both the *frzF* and *frzG* mutant strains are defective in directing cell movement through colonies. These data indicate that the transition to an organized multicellular state during predation in *M. xanthus* relies on the tactic behavior of individual cells, mediated by a Che-like signal transduction pathway.

chemotaxis | morphogenesis | predation | rippling | chemosensory

Multicellularity has emerged several times in separate lineages of life, giving rise to plants, animals, and many other multicellular species (1). In most cases the origins of multicellularity have been obscured by time, but in general it is thought to arise through a gradual process of increasing cooperative traits between sister cells of the same organism. Many bacterial species also show multicellular organization in colony architecture or biofilm ultrastructure (2, 3). In bacteria, multicellularity is often induced by specific environmental conditions rather than as a function of programmed growth. In this report, we examine how the predatory bacterium, *Myxococcus xanthus* reorganizes its multicellular structure after invading a colony of suitable *Escherichia coli* prey.

M. xanthus is capable of forming several distinct multicellular structures (4). *M. xanthus* cells are motile on solid surfaces through gliding as a combination of individuals and groups ranging from 2 to 3 cells up to 10^3 cells in a cohesive pack. Gliding movement is driven by a combination of polar type IV pili and distributed focal adhesion sites (5–7). Under conditions of high cell density, *M. xanthus* cells form fruiting body aggregates of $\approx10^5$-10^6 cells. Within fruiting bodies, low-nutrient availability induces vegetative rods to differentiate into nonmotile spores (8). During predation, *M. xanthus* cells organize into rippling wave structures. Rippling behavior coordinates cell movement across areas of several square millimeters and can involve $>10^8$ cells working as a unit.

Multicellular rippling in *M. xanthus* is a phenomenon that is superficially similar to many patterns displayed by other biological and chemical systems (9). Yet, it is unique in that counter migrating cells reflect off each other producing a convective- rather than diffusion-based wave pattern (10). One model is that rippling constitutes an intermediate phase of cell organization before a more permanent fruiting body structure (11). However, rippling is not observed under all conditions that promote fruiting body formation (12). Additionally, rippling is induced by *M. xanthus* during predation on a variety of microbial species or degradation of macromolecular growth substrates such as peptidoglycan, protein, and chromosomal DNA (13, 14). An alternative hypothesis is that rippling occurs as a result of directed cell

movement to enhance contact with prey macromolecules to facilitate predation.

In swimming *E. coli* cells, individuals find optimal positions within spatial gradients of chemoeffectors by altering their behavior (smooth swimming and tumbling), a process controlled by the chemotaxis (Che) signal transduction pathway (15). Nonchemotactic mutants are less competent than chemotactic strains in both capillary assays and infection models (16, 17). Each individual cell makes decisions on the basis of its own perception of the local chemical environment, yet complex multicellular patterns can emerge, including expanding swarm rings and focal aggregates (18, 19). Chemical signals are sensed through an array of chemoreceptors and the signal is transduced to the flagellar motors to control the swimming behavior of cells (20). The sensitivity of the receptors in Che-like signal transduction is subject to methylation via the opposing biochemical activities of the methyltransferase (CheR) and methylesterase (CheB). Altering the sensitivity of the receptors allows cells to adapt their behavior to subtle changes across a wide range of chemical concentrations. *E. coli cheR* and *cheB* mutants are ineffective at directing cell movement through chemical gradients as cells are locked in either a constitutively smooth swimming or a constitutively tumbly behavioral state (15).

In *M. xanthus*, the Che-like Frz pathway has previously been shown to regulate the frequency at which cells change the leading pole during surface gliding, similar to regulation of flagellar rotation in *E. coli* (21). Therefore, if predatory rippling in *M. xanthus* depends on the behavior of individuals similar to that seen during *E. coli* chemotaxis, then we predict that the Frz pathway will be required for controlling this behavior. If this hypothesis is correct, *M. xanthus* cells should display the two hallmarks of bacterial chemotactic behavior during predatory rippling: directed movement and adaptation to a stimulus.

Results

Directed Movement During Cellular Reorganization to Rippling. To analyze predatory behavior we make use of *M. xanthus* strain DZ2, which has a low intrinsic level of autolysis and *E. coli* strain β2155, which is a diaminopimelic acid (DAP) auxotroph whose growth is restricted in the absence of DAP, allowing us to analyze *M. xanthus* behavior in relation to an unchanging source of prey. During predation assays, *M. xanthus* cells organize into dramatically different structures depending on whether they are inside or outside of the prey colony (Fig. 1*A*). In the absence of prey, *M. xanthus* cells glide in amorphous groups such that no stable pattern of organization can be observed after 1 h of incubation (Fig. 1*B*). In contrast, cells within the prey colony organize into dynamic, parallel rippling waves and maintain this organization over time (Fig. 1*C*). In both the presence and absence of prey, cells are actively motile and glide at similar velocities: 2.7 +/−
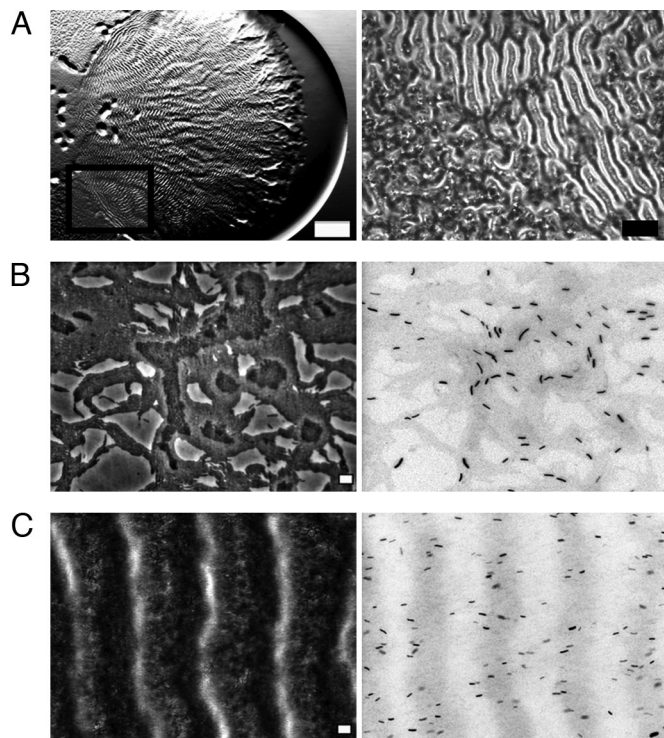
MICROBIOLOGY

Fig. 1. Multicellular reorganization during predation. (*A*) Stereo microscopy (*Left*) of *M. xanthus* strain DZ2 penetrating an *E. coli* prey colony and inducing rippling behavior. The image is centered on the prey colony, where a majority of the prey cells have been lysed and are no longer visible, but a fraction of the remaining *E. coli* colony is visible as a dark crescent on the Right edge. The open box denotes the area of the phase contrast image (*Right*) which is centered on the near edge of the prey colony where the transition from nonrippling to rippling behavior can be observed. (White scale bar, 1 mm; Black scale bar, 100 μm.) (*B*) Phase contrast (Left) and fluorescence microscopy (Right) of DZ2 mixed in a 50:1 ratio with GFP-labeled DZ10547, showing the characteristic mesh pattern of *M. xanthus* gliding behavior in the absence of prey. (*C*) Within the prey colony, the rippling pattern is stably maintained, although individual cells change position. (White scale bars in *b* and *c*, 10 μm.)

0.9 μm/min in the absence of prey and 2.8 +/− 0.7 μm/min in the presence of prey.

To determine whether *M. xanthus* cells display directed movement during predatory rippling, *M. xanthus* strain DZ2 was mixed with a strain carrying GFP fused to the highly expressed *pilA* promoter and fluorescence microscopy was performed in the presence and the absence of prey [Fig. 1 *B* and *C* and supporting information (SI) Movies 1 and 2]. Tracking of cells was performed by mixing DZ2 cells with GFP-labeled cells on an agar-covered microscope slide and indicates that in the absence of prey, *M. xanthus* cell movement occurs in curved trajectories, with changes of direction occurring gradually through cell bending and collisions with other cells, rather than through oscillation of the leading cell pole (Fig. 2*A*). Net movement of cells was analyzed by plotting the total displacement of 100 individual cell displacement vectors after 30 min of movement (Fig. 2*A*). Net displacement occurs in all directions, with various magnitudes, and the multicellular makeup of the group consists of an amorphous pattern with no relationship to the initial pattern in the absence of prey stimuli (Fig. 1).

Previous studies on cell behavior during rippling led to the conclusion that there is no net cell displacement, i.e., no directed movement (22). However, those experiments were performed in closed systems where the ripple-inducing substrate was distributed throughout the sample. To examine rippling behavior in an open system, *M. xanthus* strain DZ2 cells were mixed with
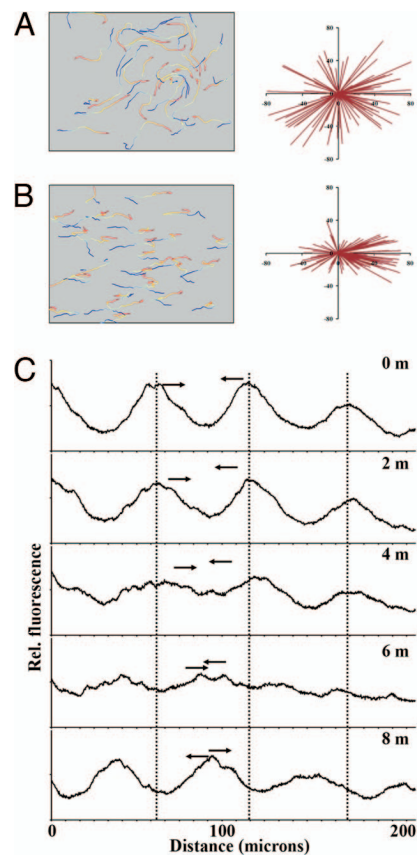

Fig. 2. Tracking movement of *M. xanthus* cells. Tracking of GFP-labeled cells in (*A*) the absence of prey and (*B*) the presence of *E. coli* prey. Experimental setup is the same as in Fig. 1. Thirty cell tracks are shown for each condition. Cell movement over time is represented by the change in color of each track, with the beginning of the track labeled in dark blue and the end in dark red. Vector displacements of 100 cells for each condition are shown on the Right. The direction of migration through the *E. coli* prey colony is from Left to Right. (*C*) Distribution of cells was monitored at 2-min intervals by measuring fluorescence intensity across the entire field of view. The dashed line indicates the position of the wave crests at 0 min, and the arrows show the general direction of cell movement in the given area. The wave structure dissipates as *M. xanthus* cells leave the initial wave aggregates, but a similar pattern of aggregation emerges, shifted by ½ wavelength, at 8 min.

GFP-labeled cells and pipetted adjacent to an *E. coli* strain β2155 prey colony on an agar-covered microscope slide. *M. xanthus* ripples can be observed as dense bands of autofluorescence that aggregate and dissipate in a synchronized, oscillating manner with a period of ≈8 min (Figs. 1*C* and 2*C*). New ripple aggregates that form are shifted by ≈½ wavelength relative to the previous ripple crests (Fig. 2*C*). Analysis of individual cell behavior indicates that movement occurs along primarily linear paths that are perpendicular to the orientation of the multicellular ripple structure (compare Figs. 1*C* and 2*B*). Thus, there is little movement in the *y*-axis and cells are constrained to moving along a nearly one-dimensional path. Both the direction and magnitude of the displacement vectors are biased to the positive *x*-axis, the direction of swarm migration through the *E. coli* prey colony. Thus, although rippling behavior can last for days, the individual structures survive only for a few minutes and seem to be indicative of a shifting equilibrium of *M. xanthus* cell density rather than the intermediate construction of a larger multicellular structure.

Adaptation to Prey Stimuli. Although rippling is a stable multicellular behavior, it takes time for the cells to coalesce into waves
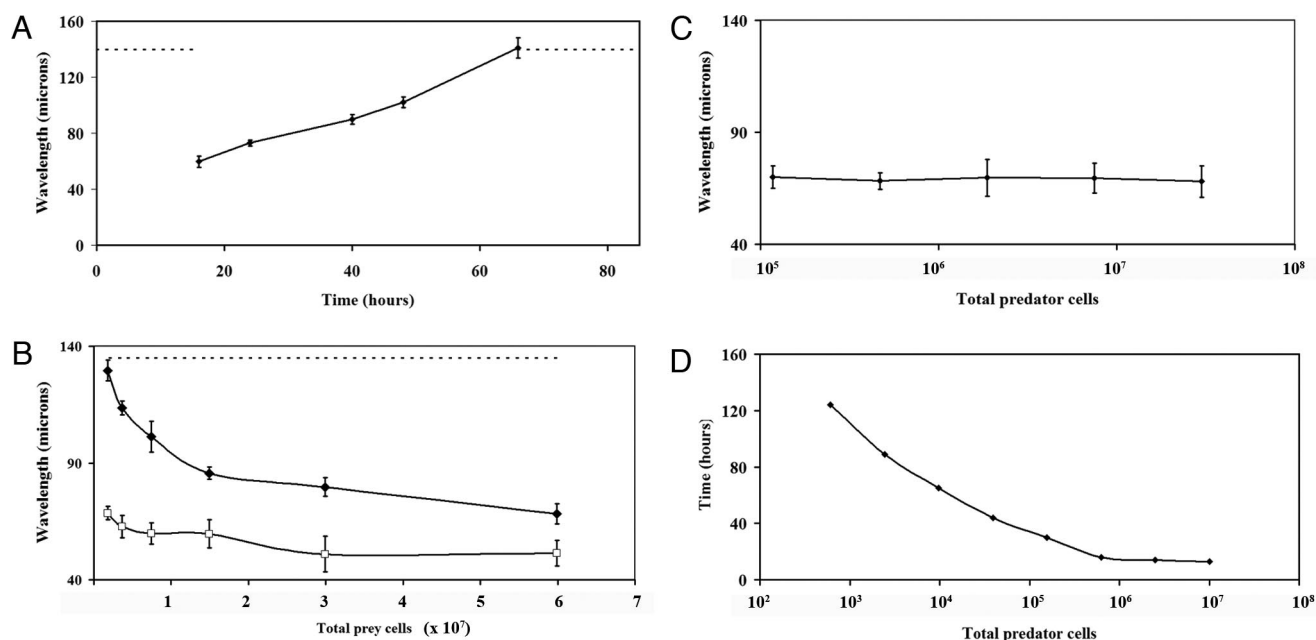
Fig. 3. Quantitative analysis of rippling pattern dynamics. (*A*) Rippling wavelength as a function of incubation time during predation. A 1-μl suspension of 10^6 total *M. xanthus* strain DZ2 cells pipetted onto CFL media adjacent to a 3-μl colony containing 5×10^7 cells of *E. coli* β2155 prey. The dashed line indicates times when quantifiable rippling was not observed. (*B*) Rippling wavelength at 40 h changes as a function of *E. coli* β2155 prey cell density (2×10^6 to 6×10^7 total cells) in *M. xanthus* strain DZ2 (diamonds), the wavelength is constitutively short in $\Delta frzG$ (open sqaures), and no rippling is observed in $\Delta frzF$ (−). (*C*) Rippling wavelength shows no change as a function of *M. xanthus* strain DZ2 cell density at 40 h (2×10^5 to 4×10^7 total cells) incubated with 5×10^7 cells of *E. coli* β2155 prey. (*D*) Rippling induction time changes as a function of *M. xanthus* strain DZ2 cell density (6×10^2 to 1×10^7 total cells) incubated with 5×10^7 cells of *E. coli* β2155 prey.
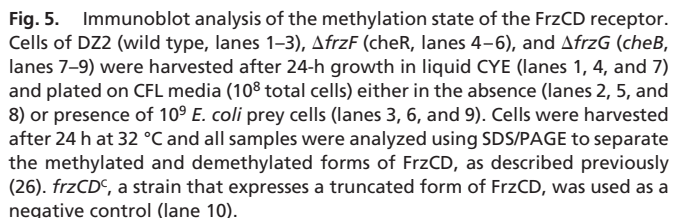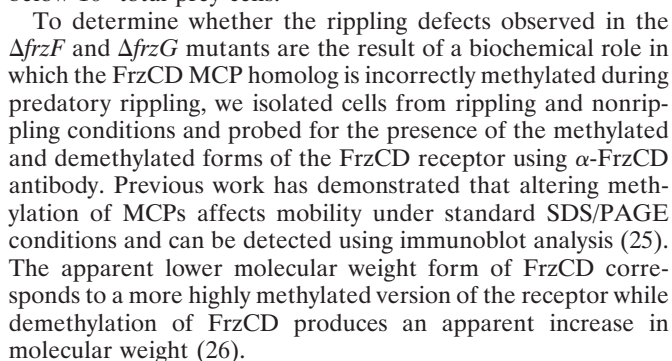
and rippling terminates soon after the available prey macromolecules have been consumed, such that rippling behavior lasts for a finite interval. To determine whether changes occur throughout the duration of rippling behavior, *M. xanthus* cells were pipetted adjacent to *E. coli* cells on a cloned fruiting light (CFL) low-nutrient agar plate and the distance between wave crests was measured from the beginning to the end of predation (Fig. 3*A*). There is entry of *M. xanthus* cells into the prey colony, but no measurable rippling during the first 18 h of the assay. After initiating, the ripples display a short wavelength of ≈ 60 μm. There is a gradual increase from 18 to 66 h in the wavelength of the ripples with a maximum wavelength of 140 μm. After 66 h, rippling behavior was still occasionally observed in scattered areas of the colony, but was not quantifiable.

To determine whether changes in rippling behavior occur over time as a result of adaptation by *M. xanthus* cells to the gradual loss of prey, predation assays were performed in which various levels of prey were provided, while the initial *M. xanthus* cell density was held constant (For quantification see Fig. 3*B*, for images see Fig. 4*C*). High densities of prey stimulate formation of a large quantity of ripples with a short wavelength between crests. Lower cell densities of prey result in longer wavelengths until a threshold is reached at which rippling is no longer observed. The output wavelength observed during rippling ranges from 70 to 135 μm, consistent with the changes observed over time (Fig. 3*A*). It is expected that the presence of prey will also cause a gradual increase in the *M. xanthus* cell density as the prey are consumed and the *M. xanthus* cells grow and divide. Thus the changes in wavelength observed could be due, in part, to increasing predator cell density. To determine whether the *M. xanthus* cell density also impacts the rippling wavelength, we performed similar assays in which the predator cell density was varied, while the prey cell density was held constant (Fig. 3*C*). Changes in the initial *M. xanthus* cell density have little effect on

the output wavelength of rippling. At the cell densities tested, no significant change in ripple wavelength was observed.

Although the predator cell densities tested had no effect on ripple spacing, analysis of a wider range of initial cell densities indicates that the cell density of *M. xanthus* is critical for the timing of rippling induction. Fig. 3*D* shows the average time required for 10 parallel waves to appear. The resulting curve is biphasic, with a steep slope below 5×10^5 cells and a shallow curve at higher cell densities. This indicates that at predator densities at and above 5×10^5 cells, rippling is able to initiate rapidly, with the only delay being the result of factors such as biosynthesis of motility organelles, sensing of prey, and the time required to reorganize into ripples. At lower predator densities there is a longer delay, which is likely the result of insufficient *M. xanthus* cell density to facilitate rippling. Taken together these results indicate that rippling wavelength is adaptable and in proportion to prey cell availability.

Molecular Controls of Adaptation. In *E. coli*, adaptation of cell motility to chemical stimuli occurs through the reversible methylation of the methyl-accepting chemotaxis proteins (MCPs) catalyzed by the methyltransferase, CheR, and the methylesterase, CheB (23). The homologs in the *M. xanthus* Frz pathway that modify the FrzCD receptor are FrzF and FrzG, respectively (20). While cells lacking FrzF reverse direction of movement very rarely in comparison to wild type, a deletion of *frzG* does not lead to any obvious defect in the reversal frequency (24). To determine the impact of the Frz pathway on multicellular structures, we examined the wild-type, $\Delta frzF$, and $\Delta frzG$ strains during gliding, fruiting body formation, and rippling behaviors (Fig. 4). During colony expansion, wild-type and $\Delta frzG$ cells glide in a meshed pattern of individuals and groups (Fig. 4*A*). In contrast, $\Delta frzF$ displays a dispersed pattern of individuals and very small groups. Under low-nutrient, high-cell-density conditions, distinct fruiting body aggregates can be observed forming in the

MICROBIOLOGY

Fig. 4. Cooperation analysis in adaptation mutants. A 10-μl aliquot containing 10^7 *M. xanthus* strain DZ2 cells was pipetted on CFL agar in the absence of prey. Stereo and phase microscopy images were captured at 72 h at (*A*) the colony edge at which group gliding behavior can be observed and (*B*) the colony center where fruiting body aggregation is observed. A Δ*frzF* mutant is defective in forming gliding groups and also forms unorganized "frizzy" aggregates. Δ*frzG* displays a phenotype with only subtle differences from the wild type in the absence of prey. (*C*) After 40 h in coculture with *E. coli* prey, wild-type cells modulate their rippling wavelength in response to the availability of prey. The Δ*frzF* mutant does not form ripple structures. The Δ*frzG* mutant forms numerous ripples at all prey cell densities in which rippling is induced. The direction of migration through *E. coli* prey is from Left to Right. (Black bar, 100 μm in *a* and *c*; White bar, 1 mm (*b*).)

Fig. 5. Immunoblot analysis of the methylation state of the FrzCD receptor. Cells of DZ2 (wild type, lanes 1–3), Δ*frzF* (cheR, lanes 4–6), and Δ*frzG* (cheB, lanes 7–9) were harvested after 24-h growth in liquid CYE (lanes 1, 4, and 7) and plated on CFL media (10^8 total cells) either in the absence (lanes 2, 5, and 8) or presence of 10^9 *E. coli* prey cells (lanes 3, 6, and 9). Cells were harvested after 24 h at 32 °C and all samples were analyzed using SDS/PAGE to separate the methylated and demethylated forms of FrzCD, as described previously (26). *frzCD*^c, a strain that expresses a truncated form of FrzCD, was used as a negative control (lane 10).

Immunoblot analysis of strain DZ2 after growth in nutrient-rich liquid medium shows that both methylated and demethylated forms of FrzCD are detectable (Fig. 5). Both forms of FrzCD were also detected when cells were incubated on a solid surface for 24 h in the absence of prey. However, in the presence of prey, FrzCD can only be detected in the methylated state. In a Δ*frzF* methyltransferase mutant, FrzCD was detected constitutively in the demethylated state under the three conditions tested (Fig. 5, lanes 4–6). In a Δ*frzG* methylesterase mutant, the FrzCD protein was detected primarily in the methylated state (Fig. 5, lanes 7–9). Together, these data indicate that the presence of prey can alter the methylation state of the FrzCD receptor and that both the FrzF and FrzG proteins are required to modify the FrzCD methylation state to bring about adaptation in response to prey.

Adaptation Components Are Essential in a Predatory Taxis Assay. *E. coli cheB* and *cheR* mutants have opposite behavioral phenotypes; *cheB* is tumbly and *cheR* is smooth swimming. Yet, both mutants are defective in their ability to direct movement in various chemotaxis assays (15, 27, 28). Similarly, the Δ*frzF* and Δ*frzG* mutants show opposite phenotypes with respect to rippling behavior; Δ*frzF* does not ripple, whereas Δ*frzG* ripples at a constitutively short wavelength. To determine the effect of these mutations on general predation ability, we devised a predatory taxis assay. In this assay, *M. xanthus* cells are pipetted into the center of a long strip of *E. coli* prey cells and the swarm expansion is measured in the dimension containing prey (*x*-axis) and the dimension lacking prey (*y*-axis) (Fig. 6*A*). In the absence of prey, *M. xanthus* strain DZ2 expands uniformly at a rate of ≈100 μm/h (Fig. 6*B*). This rate is constant across a wide range of basal nutrient levels (0.01–10 g/liter casitone). In the presence of prey, the rate of swarm expansion in wild type is unchanged during the first 24 h when rippling is not observed. Soon after rippling induction, swarm expansion increases to a rate of ≈190 μm/h. In a Δ*frzG* mutant the rate of swarm expansion is ≈100 μm/h both in the presence and absence of prey, even after the induction of rippling behavior (Fig. 6*C*). In the Δ*frzF* mutant, swarm expansion is maintained at ≈100 μm/h in the presence of prey. In the absence of prey, the rate of swarm expansion of Δ*frzF* begins at 100 μm/h during the first 24 h but decreases over time to a rate of 50 μm/h during the last 24 h of the assay (Fig. 6*D*). Together, these data indicate that adaptation via methylation of FrzCD is required for directed movement during predation.

Discussion

During bacterial chemotaxis, the methylation state of the receptors is regulated by the adaptation proteins CheB and CheR

wild-type and Δ*frzG* strains, but the Δ*frzF* mutant displays disorganized, frizzy aggregates of cells (Fig. 4*B*) as described previously (20). In the presence of prey, wild-type *M. xanthus* ripples in accordance with the abundance of prey (Fig. 4*C*). The Δ*frzF* mutant does not show rippling behavior at any of the prey cell densities tested. The Δ*frzG* mutant, however, shows a distinct hyperrippling phenotype, in which ripple structures are tightly packed resulting in a constitutively short output wavelength regardless of the cell density of prey provided (for quantification, see Fig. 3*B*). This hyperrippling phenotype is consistent with an inability to adapt to decreasing prey availability. Rippling was not observed in either the wild-type strain or the Δ*frzG* mutant below 10^6 total prey cells.

To determine whether the rippling defects observed in the Δ*frzF* and Δ*frzG* mutants are the result of a biochemical role in which the FrzCD MCP homolog is incorrectly methylated during predatory rippling, we isolated cells from rippling and nonrippling conditions and probed for the presence of the methylated and demethylated forms of the FrzCD receptor using α-FrzCD antibody. Previous work has demonstrated that altering methylation of MCPs affects mobility under standard SDS/PAGE conditions and can be detected using immunoblot analysis (25). The apparent lower molecular weight form of FrzCD corresponds to a more highly methylated version of the receptor while demethylation of FrzCD produces an apparent increase in molecular weight (26).
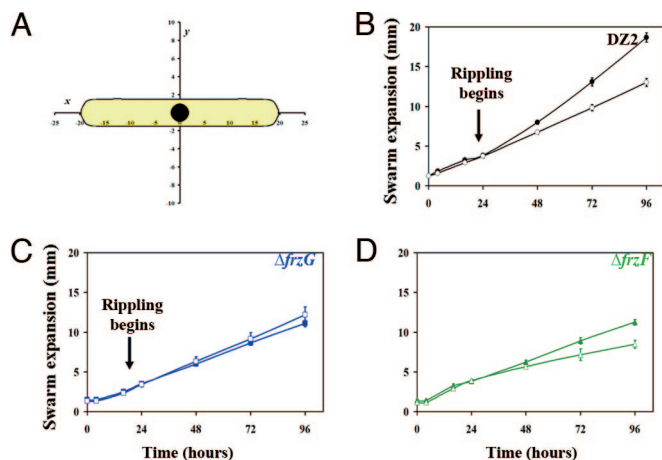
Fig. 6. Tactic assay of predatory behavior. A 1-μl aliquot containing 10^6 *M. xanthus* cells was pipetted in the center of a 40 × 2.5 mm strip of *E. coli* β2155 containing a total of 4 × 10^8 cells. Swarm expansion was measured in two axes; the x-axis contains prey cells (closed shapes), the y-axis does not (open shapes). The arrows indicate when rippling behavior begins. (*A*) Assay diagram, (*B*) *M. xanthus* strain DZ2, (*C*) Δ*frzG*, and (*D*) Δ*frzF*.

and provides a molecular memory that allows cells to compare the current signal to the recent past and adjust their behavior accordingly (23). Recently, Che-like pathways have been shown to control processes other than chemotaxis including biofilm formation, spore cell differentiation, and flagella biosynthesis (29–31). Here, we show that a Che-like mechanism is used by *M. xanthus* cells to navigate through prey colonies and causes the formation of transient multicellular rippling structures during predation. We refer to this behavior as predataxis, as the behavior of *M. xanthus* cells during predation is a novel example of how bacteria can regulate cell movement in response to a complex environment.

There are three main points to consider when comparing directed movement during predation by *M. xanthus* to the results from more conventional chemotactic assays on *M. xanthus* gliding. One, chemotaxis assays use soft 0.3% agar, on which cells glide more rapidly relative to the 1.5% agar used in the predation assays described here (32, 33). Two, no small molecule has yet been identified that can induce rippling behavior, although several nondiffusing macromolecules such as peptidoglycan and chromosomal DNA can (13, 14). Three, several chemical effectors on *M. xanthus* movement have been identified. Chemorepellents, such as isoamyl alcohol, cause individual *M. xanthus* cells to hyperreverse (34, 35). Chemoattractants such as phosphatidyl ethanolamine (PE) derivatives with specific fatty acid side chains can elicit a positive chemotaxis response and cause individual cells to inhibit reversals (32, 36). It is surprising then, that during predation a positive tactic response is observed in combination with an *increase* in cellular reversals. Taken together, these data indicate that the ability of *M. xanthus* cells to navigate through a nondiffusing colony of suitable prey is fundamentally different from the way cells respond to small molecules.

On the basis of the observed individual *M. xanthus* cell velocity average of 2.8 ± 0.7 μm/min, the maximum rate of swarm expansion should be in the range of 60–105 μm/h if cell movement is random. We observed that swarm expansion occurs at a rate of ≈100 μm/h in the absence of prey, but increases to as much as 190 μm/h in the presence of prey. Because no significant increase in the velocity of individual cells was observed after rippling induction, the increased rate of swarm expansion in the direction of prey must be the result of the inhibition of random cell movement, allowing cells to dedicate

nearly all of their potential velocity (120–205 μm/h if there are no reversals) into vectors oriented toward more prey.

Individual *M. xanthus* cells move more slowly than *M. xanthus* groups, and this may prevent a single cell from rapidly traversing the entire prey colony on its own. Thus, we explain the emergence of rippling behavior as a balance between two constraints—maintaining contact with neighboring *M. xanthus* cells to achieve maximum gliding velocity, balanced with an impetus to maintain contact with prey cells for maximum feeding potential. Cells that move "forward" through a prey colony will inevitably distance themselves from their peers, in which case these cells would benefit from a reversal of the leading cell pole. Cells that move "backward" through a prey colony will eventually lose contact with prey as they move toward a higher density of *M. xanthus* cells, again leading to a benefit from a cell reversal. The combination of these two pressures could explain the formation and rapid dissolution of wave structures during predation.

M. xanthus demonstrates a number of cooperative traits including cell density-dependent macromolecule degradation, cell–cell exchange of motility components, and a higher efficiency of prey cell lysis when rippling is observed (11, 14, 37, 38). Yet, the formation of ripples alone is insufficient for maximum predation, because the Δ*frzG* mutant is competent for rippling, yet defective at increasing swarm expansion through a prey colony. Thus, cooperative group behavior in *M. xanthus* occurs against a backdrop of the tactic behavior of individuals.

Methods

Strain Handling. *M. xanthus* strains DZ2 (wild type), DZ4483 (Δ*frzF*), DZ4482 (Δ*frzG*), DZ4486 (*frzCD*^{C}), and DZ10547 (*pilA::gfp/pilA+*) were used in this study (24, 39). *E. coli* strain β2155 was used as prey (40). For routine culturing, *M. xanthus* was grown in CYE broth and *E. coli* in LB broth (24, 41). Kanamycin was supplied when appropriate at 100 μg/ml and DAP at 150 μg/ml. CFL agar was used for analysis of *M. xanthus* cells under low-nutrient conditions (8). Ten millimolar MOPS, pH 7.6 buffer was used for harvesting and washing of cells.

Cell Tracking. Microscope slides were prepared with rubber gaskets loaded with a 750-μl volume of CFL media solidified with 1.0% agarose. One microliter of *M. xanthus* (10^6 total cells) and 3 μl of *E. coli* (5 × 10^7 total cells) were added to the agarose pad and incubated at 32 °C. *M. xanthus* strain DZ2 was mixed with DZ10547 50:1 in the absence of prey and 200:1 in the presence of prey. For microscopy, cover slips were added to the slides to prevent evaporation and time-lapse pictures were captured at 1-min intervals for 30–60 min. Fluorescence images were captured using a Leica microscope with the appropriate GFP filter. The exposure times were 0.5–1.5 s for the GFP signal, and 0.1 s for a phase contrast image. The images were captured by a Hamamatsu Orca C9495 camera and analyzed with QCapture Pro and Microsoft Excel software.

National Institutes of Health Image J software was used for cell tracking. For calculating net cell displacement, the coordinate positions of cells were measured after 30 min and were collected for cells that do not leave the field of view. Data were pooled from four samples from independent cultures. Cell velocities were calculated on the basis of cell displacement changes in 1-min intervals. In total >100 cells from three independent samples were analyzed for each condition.

Quantitative Analysis of Rippling Behavior. Cultures of *M. xanthus* and *E. coli* cells were harvested at mid-log phase and washed three times in 10 mM MOPS (pH 7.6) buffer. Serial dilutions of *E. coli* cultures were prepared in twofold steps ranging from 2 × 10^6 to 6 × 10^7. Serial dilutions of *M. xanthus* cultures were prepared in fourfold steps ranging from 6 × 10^2 to 4 × 10^7. Three microliters of *E. coli* culture were pipetted onto CFL plates and allowed to dry. *M. xanthus* cells were added to the edge of the *E. coli* prey colony. Plates were incubated at 32 °C for 40 h and rippling behavior was observed using a Nikon SMZ1500 stereomicroscope. The rippling wavelength for each sample was determined by measuring eight consecutive waves in three separate areas of the colony (24 wavelengths total). Assays were performed a minimum of three times, with representative images selected in each case. Images were captured using a QImaging MicroPublisher 5.0 RTV CCD camera and QCapture Pro software. Images were compiled into movies with Microsoft Moviemaker.

Immunoblotting. Overnight cultures of *M. xanthus* were harvested and an aliquot was pelleted and saved at −20 °C as a control. The remaining cells were

washed twice and 10^8 *M. xanthus* cells were spread on CFL plates either with or without 10^9 *E. coli* strain β2155 cells. Plates were incubated for 24 h at 32 °C. Rippling behavior was confirmed and cells were harvested from plates. Cells were resuspended in TE buffer and sonicated. The soluble protein fraction was normalized to 5 μg/ml using Bio-Rad protein assay, boiled in SDS and separated using SDS/PAGE. Protein was transferred to polyvinylidene fluoride (PVDF) membranes and detected using anti-FrzCD antibody (primary) used at 1/10,000 and anti-IgG (rabbit)-HRP conjugate (secondary) at 1/15,000, similar to previously described method (21).

Predataxis Assay. Forty microliters containing 4×10^8 *E. coli* β2155 cells were pipetted in 2 μl adjacent aliquots to generate a thin strip of prey with dimensions of 20 mm × 2.5 mm on a CFL agar plate. A 1-μl aliquot containing ≈10^6 *M. xanthus* cells was pipetted in the center of the prey strip. Swarm expansion was measured at the time indicated in two axes; the long axis of the *E. coli* strip is treated as the *x*-axis and the short axis as the *y*-axis. Measurements were collected from three independent samples for each strain.

1. King N (2004) The unicellular ancestry of animal development. *Dev Cell* 7:313–325.
2. Aguilar C, Vlamakis H, Losick R, Kolter R (2007) Thinking about *Bacillus subtilis* as a multicellular organism. *Curr Opin Microbiol* 10:638–643.
3. Camilli A, Bassler BL (2006) Bacterial small-molecule signaling pathways. *Science* 311:1113–1116.
4. Zusman DR, Scott AE, Yang Z, Kirby JR (2007) Chemosensory pathways, motility and development in *Myxococcus xanthus*. *Nat Rev Microbiol* 5:862–872.
5. Mignot T, Merlie JP, Jr, Zusman DR (2005) Regulated pole-to-pole oscillations of a bacterial gliding motility protein. *Science* 310:855–857.
6. Mignot T, Shaevitz JW, Hartzell PL, Zusman DR (2007) Evidence that focal adhesion complexes power bacterial gliding motility. *Science* 315:853–856.
7. Sliusarenko O, Zusman DR, Oster G (2007) The motors powering A-motility in *Myxococcus xanthus* are distributed along the cell body. *J Bacteriol* 189:7920–7921.
8. Berleman JE, Kirby JR (2007) Multicellular development in *Myxococcus xanthus* is stimulated by predator-prey interactions. *J Bacteriol* 189:5675–5682.
9. Igoshin OA, Mogilner A, Welch RD, Kaiser D, Oster G (2001) Pattern formation and traveling waves in myxobacteria: Theory and modeling. *Proc Natl Acad Sci USA* 98:14913–14918.
10. Sliusarenko O, Neu J, Zusman DR, Oster G (2006) Accordion waves in *Myxococcus xanthus*. *Proc Natl Acad Sci USA* 103:1534–1539.
11. Stevens A, Sogaard-Andersen L (2005) Making waves: Pattern formation by a cell-surface-associated signal. *Trends Microbiol* 13:249–252.
12. Kuner JM, Kaiser D (1982) Fruiting body morphogenesis in submerged cultures of *Myxococcus xanthus*. *J Bacteriol* 151:458–461.
13. Shimkets LJ, Kaiser D (1982) Induction of coordinated movement of *Myxococcus xanthus* cells. *J Bacteriol* 152:451–461.
14. Berleman JE, Chumley T, Cheung P, Kirby JR (2006) Rippling is a predatory behavior in *Myxococcus xanthus*. *J Bacteriol* 188:5888–5895.
15. Baker MD, Wolanin PM, Stock JB (2006) Signal transduction in bacterial chemotaxis. *Bioessays* 28:9–22.
16. Mesibov R, Adler J (1972) Chemotaxis toward amino acids in *Escherichia coli*. *J Bacteriol* 112:315–326.
17. Stecher B, *et al.* (2004) Flagella and chemotaxis are required for efficient induction of *Salmonella enterica* serovar Typhimurium colitis in streptomycin-pretreated mice. *Infect Immun* 72:4138–4150.
18. Budrene EO, Berg HC (1991) Complex patterns formed by motile cells of *Escherichia coli*. *Nature* 349:630–633.
19. Budrene EO, Berg HC (1995) Dynamics of formation of symmetrical patterns by chemotactic bacteria. *Nature* 376:49–53.
20. Francis NR, Wolanin PM, Stock JB, Derosier DJ, Thomas DR (2004) Three-dimensional structure and organization of a receptor/signaling complex. *Proc Natl Acad Sci USA* 101:17480–17485.
21. McBride MJ, Weinberg RA, Zusman DR (1989) ''Frizzy'' aggregation genes of the gliding bacterium *Myxococcus xanthus* show sequence similarities to the chemotaxis genes of enteric bacteria. *Proc Natl Acad Sci USA* 86:424–428.
22. Sager B, Kaiser D (1994) Intercellular C-signaling and the traveling waves of *Myxococcus*. *Genes Dev* 8:2793–2804.

23. Hazelbauer GL, Falke JJ, Parkinson JS (2008) Bacterial chemoreceptors: High-performance signaling in networked arrays. *Trends Biochem Sci* 33:9–19.
24. Bustamante VH, Martinez-Flores I, Vlamakis HC, Zusman DR (2004) Analysis of the Frz signal transduction system of *Myxococcus xanthus* shows the importance of the conserved C-terminal region of the cytoplasmic chemoreceptor FrzCD in sensing signals. *Mol Microbiol* 53:1501–1513.
25. DeFranco AL, Koshland DE, Jr (1980) Multiple methylation in processing of sensory signals during bacterial chemotaxis. *Proc Natl Acad Sci USA* 77:2429–2433.
26. McCleary WR, McBride MJ, Zusman DR (1990) Developmental sensory transduction in *Myxococcus xanthus* involves methylation and demethylation of FrzCD. *J Bacteriol* 172:4877–4887.
27. Parkinson JS (1976) cheA, cheB, and cheC genes of *Escherichia coli* and their role in chemotaxis. *J Bacteriol* 126:758–770.
28. Yonekawa H, Hayashi H, Parkinson JS (1983) Requirement of the cheB function for sensory adaptation in *Escherichia coli*. *J Bacteriol* 156:1228–1235.
29. Hickman JW, Tifrea DF, Harwood CS (2005) A chemosensory system that regulates biofilm formation through modulation of cyclic diguanylate levels. *Proc Natl Acad Sci USA* 102:14422–14427.
30. Berleman JE, Bauer CE (2005) A che-like signal transduction cascade involved in controlling flagella biosynthesis in *Rhodospirillum centenum*. *Mol Microbiol* 55:1390–1402.
31. Kirby JR, Zusman DR (2003) Chemosensory regulation of developmental gene expression in *Myxococcus xanthus*. *Proc Natl Acad Sci USA* 100:2008–2013.
32. Kearns DB, Shimkets LJ (2001) Lipid chemotaxis and signal transduction in *Myxococcus xanthus*. *Trends Microbiol* 9:126–129.
33. Shi W, Zusman DR (1994) Sensory adaptation during negative chemotaxis in *Myxococcus xanthus*. *J Bacteriol* 176:1517–1520.
34. Shi W, Zusman DR (1994) Sensor/response in *Myxococcus xanthus* to attractants and repellents requires the frz signal transduction system. *Res Microbiol* 145:431–435.
35. Xu Q, Black WP, Mauriello EM, Zusman DR, Yang Z (2007) Chemotaxis mediated by NarX-FrzCD chimeras and nonadapting repellent responses in *Myxococcus xanthus*. *Mol Microbiol* 66:1370–1381.
36. Curtis PD, Geyer R, White DC, Shimkets LJ (2006) Novel lipids in *Myxococcus xanthus* and their role in chemotaxis. *Environ Microbiol* 8:1935–1949.
37. Rosenberg E, Keller KH, Dworkin M (1977) Cell density-dependent growth of *Myxococcus xanthus* on casein. *J Bacteriol* 129:770–777.
38. Nudleman E, Wall D, Kaiser D (2005) Cell-to-cell transfer of bacterial outer membrane lipoproteins. *Science* 309:125–127.
39. Welch R, Kaiser D (2001) Cell behavior in traveling wave patterns of myxobacteria. *Proc Natl Acad Sci USA* 98:14907–14912.
40. Dehio C, Meyer M (1997) Maintenance of broad-host-range incompatibility group P and group Q plasmids and transposition of Tn5 in *Bartonella henselae* following conjugal plasmid transfer from *Escherichia coli*. *J Bacteriol* 179:538–540.
41. Sambrook J, Fritsch EF, Maniatis T (1989) *Molecular Cloning: A Laboratory Manual* (Cold Spring Harbor Laboratory Press, Cold Spring Harbor, NY).